

## PROTECTION SCHEME FOR RENEWABLE ENERGY SOURCES BASED SMARTGRID USING STOCKWELL TRANSFORM AND RULE-BASED DECISION TREE

YOGESH MEHTA<sup>1</sup> & RAVINDRA PRAKASH GUPTA<sup>2</sup>

<sup>1</sup>Department of Electronics and Communications Engineering, Gyan Vihar University, Jaipur, Rajasthan, India

<sup>2</sup>Department of Electronics and Communications Engineering, Manda Institute of Technica, Bikaner, Rajasthan India

### ABSTRACT

The security of smart grid is under threat due to sophisticated intrusion and imperceptible faults. To make the smart grid more secure, accurate location of power system faults in the smart grid is significantly important. This accurate location of faults is a very challenging task to provide effective protection. This paper presents an effective technique for detection and classification of faults in the smart grid. The proposed technique is based on the medians of current signals calculated from the S-matrix obtained by the decomposition of current signals using Stockwell Transform. The investigated faults involve the line to ground (LG) fault, double line (LL) fault, double line to ground (LLG) fault and three phase fault involving ground (LLL). The classification of faults has been carried out with the help of rule based decision tree. The proposed technique has been tested with 100 data sets of each fault. The proposed study is carried out using IEEE-13 bus test system as a smart grid.

**KEYWORDS:** Power System Faults, Rule Based Decision Tree, Smart Grid, Stockwell Transform

### 1. INTRODUCTION

Smart grid (SG) is an electricity network, which intelligently integrates the actions of all the connected generators, including conventional and distributed generators (DG), users and consumers in order to efficiently deliver sustainable, economic and secure electricity supply to consumers. This smart grid have innovative products and services together with intelligent monitoring, control, communication, and self-healing technologies in order to (i) provide the integration and operation of generators of all sizes and technologies (ii) allow consumers to play an active role in optimizing the operation of the system (iii) significantly reduce the environmental impact of the whole electricity supply system and (iv) preserve or improve the level of system quality of service, reliability and security [1]. Faults can occur in the smart grid without early warnings due to a variety of possible causes including equipment failures, falling of trees on electrical lines, lightning strikes, animal/tree contacts, and malicious attacks. When a fault occurs in a certain region of a smart grid, some other regions of the grid may become overloaded or isolated through the tripped switchgear due to load redistribution. This continuous load redistribution often turns into a cascading phenomenon that is propagated throughout the smart grid that in turn can cause a catastrophic failure leading to a large disturbance in the smart grid [2] Hence, early detection of fault and identification of the type of fault will help in isolating the faulty section of the smart grid in order to cause the minimum damage and loss.

A wide variety of literature is reported on the smart grid and fault recognition in the smart grid. A multi-sensor feeder-level fault detection and classification algorithm based on support vector machine and the principal components has been reported in [3]. An IEEE 34-bus test system is used to implement the developed algorithm. Using the proposed

algorithm, high accuracies of fault detection and classification in the smart grids have been achieved. Manandhar et al. [4], proposed a mathematical model of smart grid systems to study pitfalls and to detect system faults/attacks, such as a DoS attack, short-term, and long-term random attacks to insure the robust security framework for the smart grid. In [5], the authors developed and validated a fast and efficient fault detection and classification algorithm considering the dynamic behavior of renewable energy sources in the smart grid. The proposed algorithm is based on the synchronised measured three-phase currents through the communication facilities available in the smart grid. A technique based on One-Class Quarter-Sphere Support Vector Machine (QSSVM) for fault detection and classification in the smart grids has been reported in [6]. In [7], the authors proposed a one bit randomized grouping algorithm to detect faults in the smart grids. An approach of big data characterization for smart grids (SGs) and its applications in fault detection, identification, and causal impact analysis is reported in [8] -[9].

This paper presents an algorithm based on Stockwell Transform and rule based decision tree for the detection and classification of power system faults in the smart grids in the presence of wind and solar PV power generations. The proposed study is carried out using an IEEE-13 bus test system modeled as smart grid. The three phase current waveforms are captured on a particular bus to calculate the proposed fault index. The proposed fault index is used to detect various types of faults in the smart grid. The investigated faults include line to ground (LG) fault, double line fault (LL) fault, double line to ground (LLG) fault and three phase fault involving ground (LLLG) in the presence of wind power system, solar power system and simultaneous presence of wind and solar power system. The proposed study has been carried out in the MATLAB/Simulink environment.

This paper is organized into six sections. Introduction is presented in the Section 1. The proposed smart grid model used for the detection of various types of the faults in the presence of wind and solar PV power generation systems has been described in the section 2. Section 3 details the proposed methodology used for the detection and classification of the various types of power system faults in the smart grid. The simulation results related to the detection of faults using Stockwell transform are presented in the section 4. The ruled decision tree based classification of the various types of faults has been described in the section 5. The performance of the proposed technique has been described in Section 6. The conclusions drawn based on the proposed study are presented in the section 7.

## **2. THE PROPOSED TEST SYSTEM OF SMART GRID**

This section describes the test system which has been utilized as smart grid incorporated with renewable energy (RE) sources such as wind and solar PV system. This is used for the detection of various types of faults in the presence of the RE sources. An IEEE-13 bus test system is modelled as a smart grid for the proposed study. The original system is a 60 Hz, 5 MVA, operating with the voltage levels of 4.16 kV and 0.48 kV. This system has the balanced and unbalanced loads and any REsource is not integrated with the original test system. The test system is modified to incorporate the wind energy conversion system (WECS) and solar PV system on the bus 680 of test system as illustrated in Figure 1. Bus 680 is considered as the point of common coupling (PCC). Doubly fed induction generator based wind energy conversion system (WECS) and solar PV system are connected to the test system at PCC through transformers T1 and T2 respectively. The loads connected to the test system at various buses are same as in the original test system. The distributed loads are connected in the middle of the respective distribution line of the test system. All the feeders of the proposed test system have the configuration 601 of the original IEEE-13 system. Lengths of line segments are same as that in the original test system. The proposed test system of smart grid is connected to the conventional generator using a substation transformer.

The transformer connected between the nodes 633 and 634 is named as T. This transformer is used to step down the voltage from 4.16 kV to 0.48 kV and bus 634 is maintained at a voltage level of 0.48 kV. Technical details of transformers are provided in the Table 1. A three phase circuit breaker is used to represent the switch between the nodes 671 and 692 of the test systems.

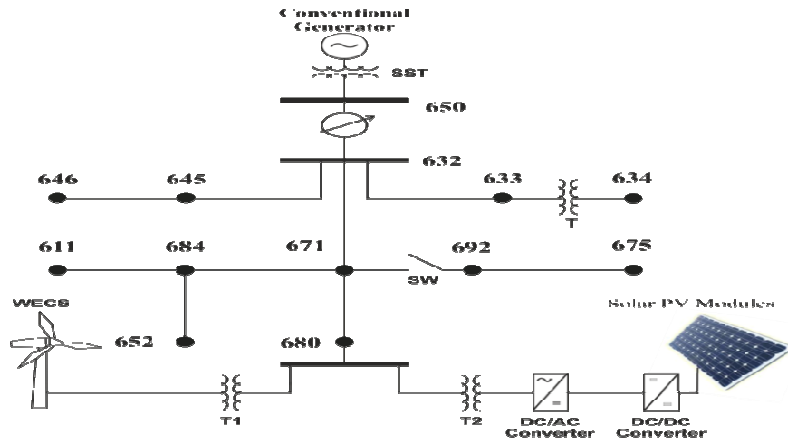


Figure 1: IEEE-13 Bus Test System Modeled as Smart Grid

Table 1

Transformer	Voltage LV Winding	Voltage HV Winding	R (pu)	X pu)
SST	4.16 kV	115 kV	0.011	0.080
T	0.48 kV	4.16 kV	0.011	0.080
T1	575 V	4.16 kV	0.380	0.070
T2	260 V	4.16 kV	0.001	0.030

### 3. PROPOSED METHODOLOGY FOR DETECTION AND CLASSIFICATION OF FAULTS IN SMART GRID

The proposed scheme used for the detection and classification of power system faults in the smart grid is shown in Figure 2. Fault in all the cases of study is created in the middle of the line connecting the buses 632 and 671 which is taken as a test location for the fault. The currents of all the three phases are captured at bus 632 of the proposed smart grid test system. The currents are decomposed using Stockwell transform (S-transform) and S-matrix is obtained. The proposed fault index is used for the detection of various faults and a feature based on standard deviation extracted from the S-matrix is used for the classification of the faults in the presence of wind and solar PV power generation in the smart grid.

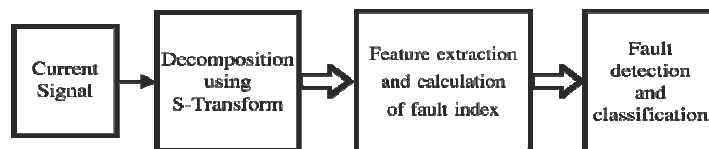


Figure 2: Proposed Scheme of Fault Detection and Classification

#### 3.1. Proposed Fault Index

A fault index is proposed to discriminate faulty phases from the healthy phases. Fault index is obtained by calculating the maximum values in each column of the S-matrix corresponding to all the investigated faults. A threshold is set to discriminate the faulty phases from the healthy phases based on the analysis of various types of faults created at various locations of the fault in the test system of smart grid. This threshold value is set to 600 for all the types of faults.

### 3.2. Stockwell's Transform

The short time Fourier Transform of a signal  $h(t)$  is defined by the following relation.

$$STFT(\tau, f) = \int_{-\infty}^{+\infty} h(t)g(\tau - t)e^{-j2\pi ft} dt$$

Where  $\tau$  and  $f$  denote the time of spectral localization and a Fourier frequency respectively, and  $g(t)$  denote a window function. The S transform can be derived from the above equation by replacing the window function  $g(t)$  with the Gaussian function as shown below.

$$g(t) = \frac{|f|}{\sqrt{2\pi}} e^{-\frac{f^2 t^2}{2}}$$

Then the S-transform is defined as

$$S(\tau, f) = \int_{-\infty}^{+\infty} h(t) \frac{|f|}{\sqrt{2\pi}} e^{-\frac{f^2(\tau-t)^2}{2}} e^{-j2\pi ft} dt$$

Hence, the S transform is a special case of the STFT with Gaussian window function. If the window of the S-transform is wider in time domain, S transform can provide better frequency resolution for lower frequency. While the window is narrower, it can provide better time resolution for higher frequency. The output of the S-transform is matrix known as an S - matrix. The information related to the frequency and amplitude of the signal can be derived from the S-matrix.

### 3.3. Rule Based Decision Tree

Rule based decision tree is based on a classification or regression model in the form of a tree structure. It divides a dataset into smaller subsets using incrementally developed decision tree based on the decision rules. The classification starts from the root node and the final result is contained in the leaf node of the decision tree. The leaf node contains the final decision of the classification.

## 4. S-TRANSFORM BASED FAULT DETECTION IN THE SMART GRID

This section presents the simulation results related to the detection of various types of faults in the smart grid using Stockwell transform used for the protection of the smart grid. Current waveform and proposed fault index of the line to ground (LG) fault, double line (LL) fault, double line to ground (LLG) fault and three phase fault involving ground (LLLG) are described in this section. Fault in all the cases of study is created in the middle of the line connecting the buses 632 and 671 which is taken as a test location for the fault creation. The faults under study are created at 10<sup>th</sup> cycle and data are recorded for 0.4 s time duration.

### 4.1. Solar PV Power Generation in Smart Grid

The solar PV plant of the capacity 1 MW is connected to the bus 680 on the smart grid test system shown in Figure 1. The solar PV system is switched on and continuously injecting power into the proposed smart grid. Detection of the various types of faults in the presence of solar PV power generation using proposed methodology is detailed in the following subsections.

#### 4.1.1. Line to Ground Fault

The line to ground fault is created in the phase A at the test location. The waveforms of currents of all the three

phases captured at bus 632 of the test system before and after the fault incident are shown in the Figure 3. It is observed that the waveforms of the healthy phases follow the same trend after the fault incident as before the fault occurrence. The faulty phase draws heavy current after the fault occurrence. The magnitude of fault current has increased by 1375 % of the magnitude in healthy condition. These current waveforms are utilized to find the fault indices for the detection of the faults or differentiating the faulty condition from the healthy condition.

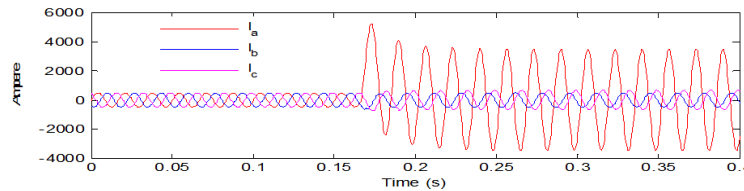


**Figure 3: Three-Phase Current at Bus-632 during LG Fault in the Presence of Solar PV Power Generation**

The variation of the proposed fault index during line to ground fault for all the three phases is shown in Figure 4. It is observed that the value of the fault index for all the phases is below the threshold value (600) nearly 250 before the fault occurrence during the healthy condition. It is also observed that the value of fault index is 1750 for the faulty phase (phase-A) after the occurrence of the fault which is higher than the threshold value. The value of fault index is less than 600 for the healthy phases (phases A & B). Hence, the healthy phases are clearly discriminated from the faulty phase. The high value of the fault index for the faulty phase will trip the respective relay to isolate the faulty section.

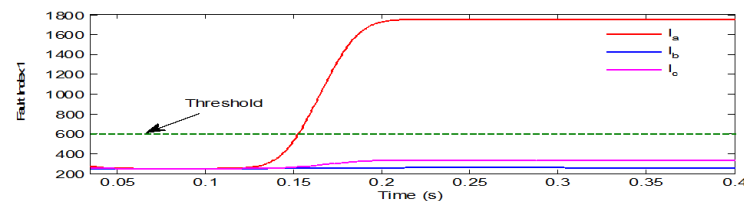


**Figure 4: Variation of Fault Indices for LG Fault In the Presence of Solar PV Power Generation**

**4.1.2. Double Line Fault**

The double line fault without the involvement of ground is created by shorting the phases A and B at the test location. The waveforms of currents of all the three phases captured at bus 632 on the test system before and after the fault incident are shown in Figure 5. It is observed that the waveform of current in the healthy phase follows the same trend after the fault incident as before the fault occurrence. The faulty phases draw heavy currents after the fault occurrence. The magnitude of fault currents has increased by 1250 % of the magnitude of current in healthy condition. These current waveforms are utilized to find the fault indices for the detection of the faults or differentiating the faulty condition from the healthy condition.

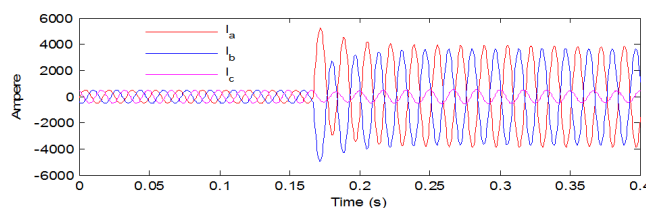


**Figure 5: Three-Phase Current at Bus-632 during LL Fault in the Presence of Solar PV Power Generation**

The variation of the proposed fault index during double fault without the involvement of fault for all the three phases is shown in Figure 6. It is observed that the value of the fault index for all the phases is below a threshold value (600) nearly 250 before the fault occurrence during the healthy condition. It is also observed that the value of fault indices is 1900 and 1800 for the faulty phases A and B respectively, after the occurrence of fault which is higher than the threshold value of 600. The value of fault index is less than 600 for the healthy phase-C. Hence, the healthy phase is clearly discriminated from the faulty phases. The high value of the fault index for the faulty phases will trip the respective relays to isolate the faulty section of the smart grid.

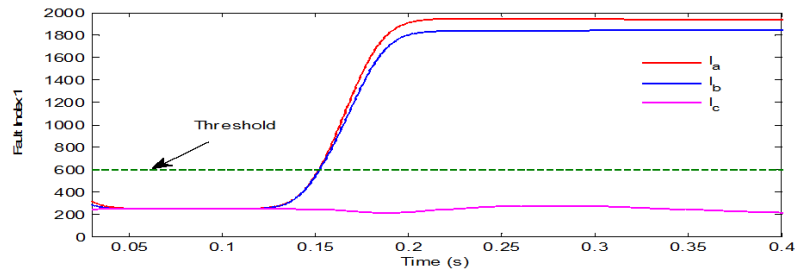


**Figure 6: Variation of Fault Indices for LL Fault in the Presence of Solar PV Power Generation**

**4.1.3. Double Line to Ground Fault**

The double line to ground fault is created by simultaneous grounding of the phases A and B at the test location. The waveforms of currents of all the three phases captured at bus 632 of the test system before and after the fault incident are shown in the Figure 7. It is observed that the waveform of current in the healthy phase follows the same trend after the fault incident as before the fault occurrence. The faulty phases draw heavy currents after the fault occurrence. The magnitude of fault currents has increased by 1500 % of the magnitude of current in healthy condition. These current waveforms are utilized to find the fault indices for the detection of the faults or differentiating the faulty condition from the healthy condition.

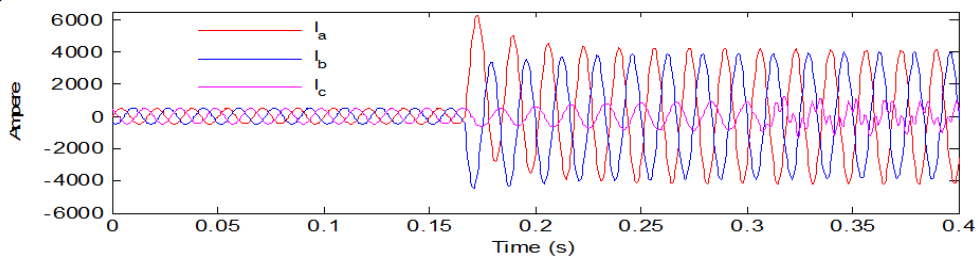


**Figure 7: Three-Phase Current at Bus-632 during LL Fault in the Presence of Solar PV Power Generation**

The variation of the proposed fault index during double line to ground fault for all the three phases is shown in Figure 8. It is observed that the value of the fault index for all the phases is below a threshold value (600) nearly equal to 250 before the fault occurrence during the healthy condition. It is also observed that the value of fault indices is 2050 and 1900 for the faulty phases A and B respectively, after the occurrence of fault which is higher than the threshold value of 600. The value of fault index is less than 600 for the healthy phase-C. However, the variations have been observed in the current of healthy phase after the occurrence of the fault. Hence, the healthy phase is clearly discriminated from the fault phases. The high value of the fault index for the faulty phases will trip the respective relays to isolate the faulty section of the smart grid.

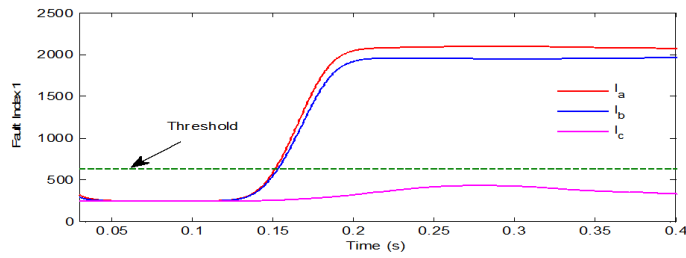


**Figure 8: Variation of Fault Indices for LLLG Fault in the Presence of Solar PV Power Generation**

**4.1.4. LLLG Fault**

The three-phase fault involving ground has been created by simultaneous grounding all the three phases at the test location. The waveforms of currents of all the three phases captured at bus 632 on the test system before and after the fault incident are shown in the Figure 9. It is observed that all the phases draw heavy currents after the fault occurrence. The magnitude of fault currents has increased by 1750 % of the magnitude of current in healthy condition. These current waveforms are utilized to find the fault indices for the detection of the fault.

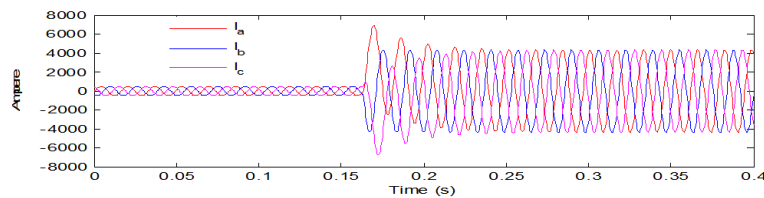


**Figure 9: Three-Phase Current at Bus-632 during LLLG Fault in the Presence of Solar PV Power Generation**

The variation of proposed fault indices during three-phase fault involving ground for all the three phases is shown in Figure 10. It is observed that the value of the fault index for all the phases is below a threshold value (600) nearly 250 before the fault occurrence during the healthy condition. It is also observed that the value of fault indices is 2200 for all the three phases after the occurrence of fault which is higher than the threshold value of 600. Hence, the three phase fault involving ground has been detected effectively and discriminated from other types of faults. The high value of fault index will trip the respective relays to isolate the faulty section of the smart grid.

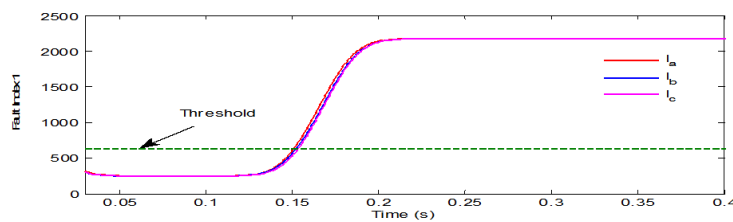


**Figure 10: Variation of Fault Indices for LLLG Fault in the Solar PV Generation**

**4.2. Wind Power Generation in Smart Grid**

The doubly fed induction generator based wind power plant of capacity 1.5 MW is connected to the bus 680 on the smart grid test system shown in Figure 1. The wind power plant switches on and continuously injecting power into the proposed smart grid. The simulation results related to detection of the various types of faults in the presence of the wind power generation using proposed methodology are described in the following subsections.

**4.2.1. LG Fault**

The line to ground fault in the presence of wind power generation is created on the phase A at the test location. The current waveforms of all the three phases captured at bus 632 on the test system before and after the fault incident are shown in the Figure 11. It is observed that the waveforms of the healthy phases follow the same trend after the fault incident as before the fault occurrence. The faulty phase draws heavy current after the fault occurrence. The magnitude of fault current has increased by 1250 % compared to the magnitude in healthy condition. These current waveforms are utilized to find the fault indices for the detection of faults or differentiating the faulty condition from the healthy condition.

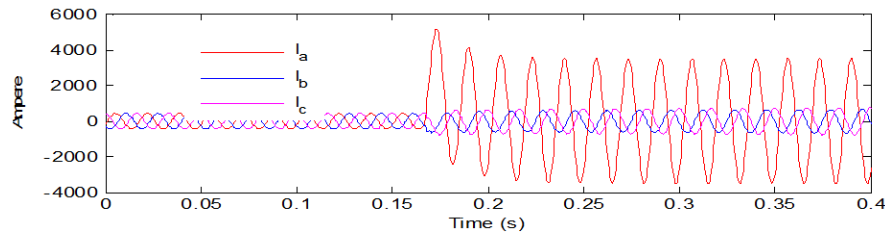


**Figure 11: Three-Phase Current at Bus-632 during LG Fault in the Presence of Wind Power Generation**

The variation of the proposed fault index during line to ground fault for all the three phases in the presence of wind power generation is shown in Figure 12. It is observed that the value of the fault index for all the phases is below a threshold value (600) nearly 250 before the fault occurrence during the healthy condition. It is also observed that the value of fault index is 1775 for the faulty phase (phase-A) after the occurrence of the fault which is higher than the threshold value. The value of fault index is less than 600 for the healthy phases (phases A & B). However, fault indices for the healthy phase increases from the 250 to 300 and 275 respectively, for the phases B and C respectively which are lower than the threshold value. Hence, the healthy phases are clearly discriminated from the fault phase. The high value of the fault index for the faulty phase will trip the respective relay to isolate the faulty section.

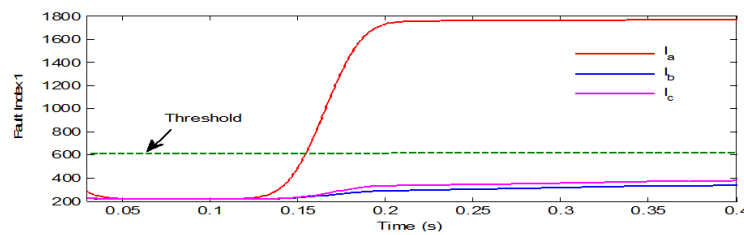


**Figure 12: Variation of Fault Indices for LG Fault in the Presence of Wind Power Generation**

**4.2.2. LL Fault**

The double line fault without the involvement of ground in the presence of wind power generation is created by shorting the phases A and B at the test location. The current waveforms of all the three phases captured at bus 632 on the test system before and after the fault incident are shown in the Figure 13. It is observed that the waveform of current in the healthy phase follows the same trend after the fault incident as before the fault occurrence. The faulty phases draw heavy currents after the fault occurrence. The magnitude of fault currents has increased by 1300 % of the magnitude of current in healthy condition. These current waveforms are utilized to find the fault indices for the detection of the faults or differentiating the faulty condition from the healthy condition.

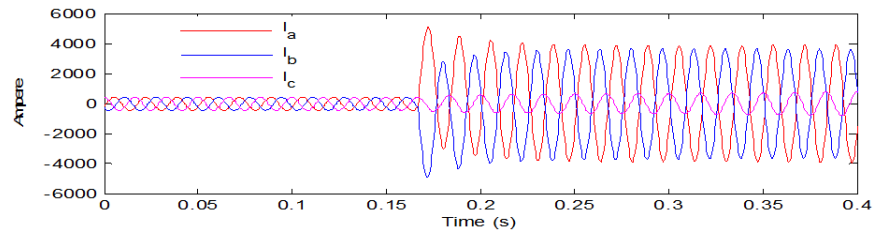


**Figure 13: Three-Phase Current at Bus-632 during LL Fault in the Presence of Wind Power Generation**

The variation of the proposed fault index during double fault without the involvement of fault for all the three phases with wind power generation is shown in Figure 14. It is observed that the value of the fault index for all the phases is below a threshold value (600) nearly 250 before the fault occurrence during the healthy condition. It is also observed that the value of fault indices is 1950 and 1850 for the faulty phases A and B respectively, after the occurrence of fault which is higher than the threshold value of 600. The value of fault index is less than 600 for the healthy phases-C. However, the fault index for the healthy phase has increased from 250 to 400 after the fault occurrence which is less than the threshold value. Hence, the healthy phase is clearly discriminated from the faulty phases. The high value of the fault index for the faulty phases will trip the respective relays to isolate the faulty section of the smart grid.

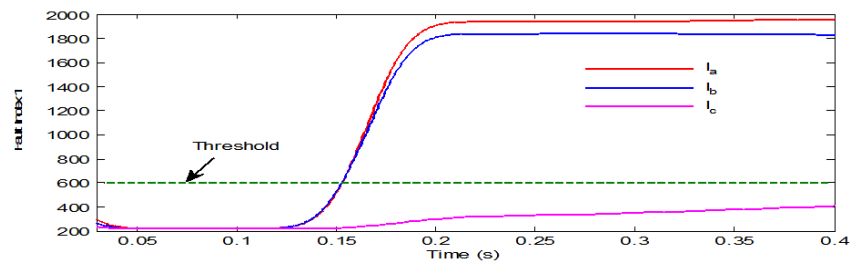


**Figure 14: Variation of Fault Indices for LL Fault in the Presence of Wind Power Generation**

#### 4.2.3. LLG Fault

The double line to ground fault in the presence of wind power generation is created by simultaneous grounding of the phases A and B at the test location. The waveforms of currents of all the three phases are captured at bus 632 on the test system before and after the fault incident are shown in the Figure 15. It is observed that the waveform of current in the healthy phase follows the same trend after the fault incident as before the fault occurrence. The faulty phases draw heavy currents after the fault occurrence. The magnitude of fault currents has increased by 1500 % of the magnitude of current in healthy condition. These current waveforms are utilized to find the fault indices for the detection of faults or differentiating the faulty condition from the healthy condition. This will also discriminate the faulty and healthy phases.

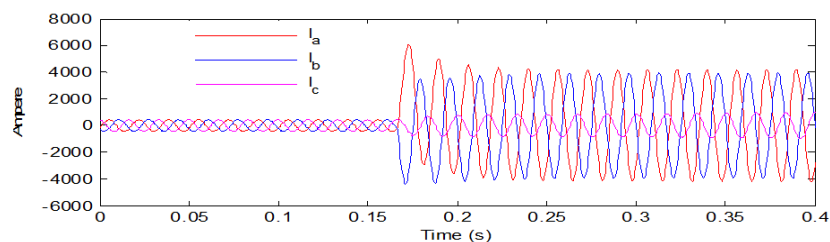


**Figure 15: Three-Phase Current at Bus-632 during LLG Fault in the Presence of Wind Power Generation**

The variation of the proposed fault index during double line to ground fault for all the three phases in the presence of wind power generation is shown in Figure 16. It is observed that the value of the fault index for all the three phases is below a threshold value (600) nearly 250 before the fault occurrence during the healthy condition. It can be observed that the value of fault indices is 2100 and 1950 for the faulty phases A and B respectively, after the occurrence of fault which is higher than the threshold value of 600. The value of fault index is less than 600 for the healthy phase-C. However, the fault index of the healthy phase also increases up to the value of 450 which is less than the threshold value. Hence, the healthy phase is clearly discriminated from the faulty phases. The high value of the fault index for the faulty phases will trip the respective relays to isolate the faulty section of the smart grid.

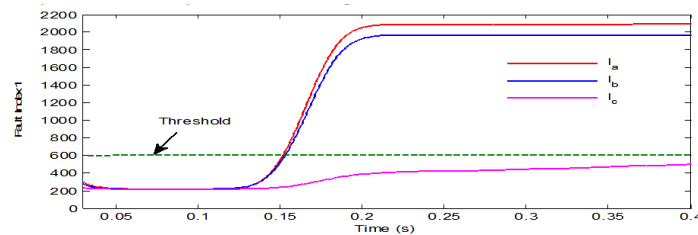


**Figure 16: Variation of Fault Indices for LLG Fault in the Presence of Wind Power Generation**

#### 4.2.4. LLLG Fault

The three-phase fault involving ground in the presence of wind power generation has been created by simultaneous grounding of all the three phases at the test location. The waveforms of currents of all the three phases captured at bus 632 on the test system before and after the fault incident are shown in the Figure 17. It is observed that all the phases draw heavy currents after the fault occurrence. The magnitude of fault currents has increased by 1800 % of the magnitude of current in healthy condition. These current waveforms are utilized to find the fault indices for the detection of the fault.

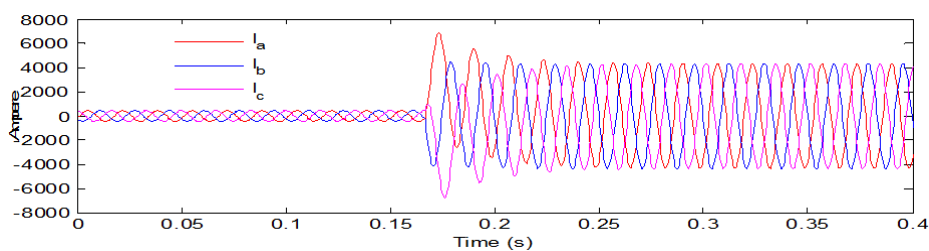


**Figure 17: Three-Phase Current at Bus-632 during LLLG Fault in the of Wind Power Generation**

The variation of proposed fault indices during three-phase fault involving ground for all the three phases with wind power generation is shown in Figure 18. It is observed that the value of the fault index for all the phases is below a threshold value (600) nearly 250 before the fault occurrence during the healthy condition. It is also observed that the value of fault indices is 2200 for all the three phases after the occurrence of fault which is higher than the threshold value of 600. Hence, the three phase fault involving ground with wind power generation has been detected effectively and discriminated from other types of faults. The high value of fault index will trip the respective relays to isolate the faulty section of the smart grid.

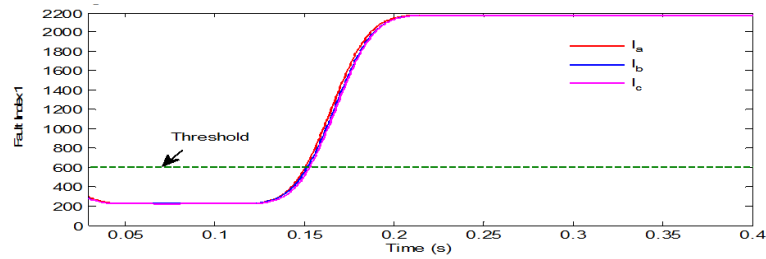


**Figure 18: Variation of Fault Indices for LLLG Fault in the Presence of Wind Power Generation**

**4.3. Simultaneous Generation of Wind and Solar PV Power in Smart Grid**

The doubly fed induction generator based wind power plant of capacity 1.5 MW and solar PV plant of capacity 1 MW are connected to the bus 680 on the smart grid test system shown in Figure 1. The wind power and solar PV plants are switched on and continuously injecting power into the proposed smart grid. The simulation results related to detection of the various types of faults in the presence of the wind power and solar PV generations using proposed methodology are described in the following subsections.

**4.3.1. LG Fault**

The line to ground fault in the simultaneous presence of wind and solar PV power generations is created in the phase A at the test location. The current waveforms of all the three phases captured at bus 632 on the test system before and after the fault incident are shown in the Figure 19. It is observed that the waveforms of the healthy phases follow the same trend after the fault incident as before the fault occurrence. The faulty phase draws heavy current after the fault occurrence. The magnitude of fault current has increased by 1400 % compared to the magnitude in healthy condition. These current waveforms are utilized to find the fault indices for the detection of faults or differentiating the faulty condition from the healthy condition.

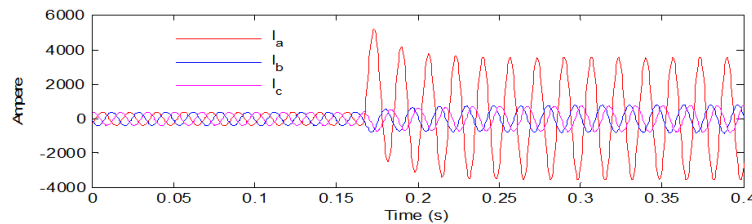


**Figure 19: Three-Phase Current at Bus-632 during LG Fault in the Simultaneous Presence of Wind and Solar Power Generations**

The variances of the proposed fault index during line to ground fault for all the three phases in the simultaneous presence of wind and solar PV power generations are shown in Figure 20. This is observed that the value of the fault index for all the phases is below a threshold value (600) nearly 250 before the fault occurrence during the healthy condition. It is also observed that the value of fault index is 1800 for the faulty phase (phase-A) after the occurrence of the fault which is higher than the threshold value. The value of fault index is less than 600 for the healthy phases (phases A & B). However, fault indices for the healthy phase increases from the 250 to 325 and 300 for the phases B and C respectively which are lower than the threshold value. Hence, the healthy phases are clearly discriminated from the faulty phase. The high value of the fault index for the faulty phase will trip the respective relay to isolate the faulty section.

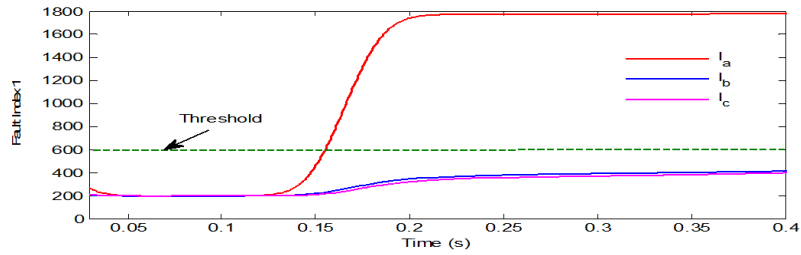


**Figure 20: Variation of Fault Indices for LG Fault in the Simultaneous Presence of Wind and Solar Power Generations**

**4.3.2. LL Fault**

The double line fault without involving the ground in the simultaneous presence of wind and solar PV power generations is created by shorting the phases A and B at the test location. The current waveforms of all the three phases captured at bus 632 on the test system before and after the fault occurrence are shown in the Figure 21. It is observed that the waveform of current in the healthy phase follows the same trend after the fault incident, as before the fault occurrence but with the continuously slight increase in the magnitude. The faulty phases draw heavy currents after the fault occurrence. The magnitude of fault currents has increased by 1200 % of the magnitude of current in healthy condition. These current waveforms are utilized to find the fault indices for the detection of the faults or differentiating the faulty condition from the healthy condition.

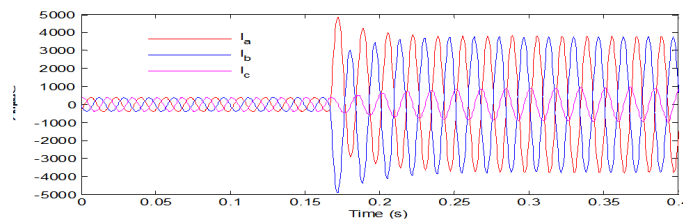


**Figure 21: Three-Phase Current at Bus-632 during LL Fault in the Simultaneous Presence of Wind and Solar Power Generations**

The variation of the proposed fault index during double line fault without the involvement of fault for all the three phases with the simultaneous generation of wind and solar PV power is shown in Figure 22. It is observed that the value of the fault index for all the phases is below a threshold value (600) nearly 250 before the fault occurrence during the healthy condition. It is also observed that the value of fault indices is 1900 for the faulty phases A and B after the occurrence of fault which is higher than the threshold value of 600. The value of fault index is less than 600 for the healthy phase-C. However, the fault index for the healthy phase has increased from 250 to 425 after the fault occurrence which is less than the threshold value. Hence, the healthy phase is clearly discriminated from the faulty phases. The high value of the fault index for the faulty phases will trip the respective relays to isolate the faulty section of the smart grid.

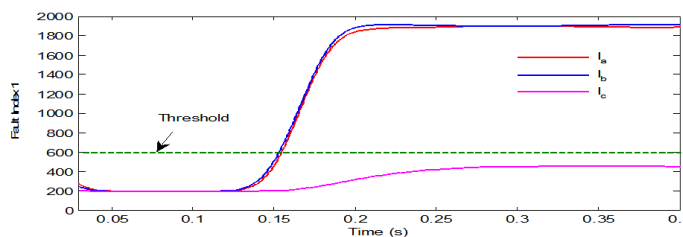


**Figure 22: Variation of Fault Indices for LL Fault in the Simultaneous Presence of Wind and Solar Power Generations**

### 4.3.3. LLG Fault

The double line to ground fault in the simultaneous presence of wind and solar PV power generations is created by simultaneous grounding of the phases A and B at the test location. The waveforms of currents of all the three phases are captured at bus 632 on the test system before and after the fault incident are shown in the Figure 23. It is observed that the waveform of current in the healthy phase has the same frequency after the fault incident, but some harmonic components are introduced and magnitude increases slightly. The faulty phases draw heavy currents after the fault occurrence. The magnitude of fault currents has increased by 1500 % of the magnitude of current in healthy condition. These current waveforms are utilized to find the fault indices for the detection of the faults or differentiating the faulty condition from the healthy condition. This will also discriminate the faulty and healthy phases.

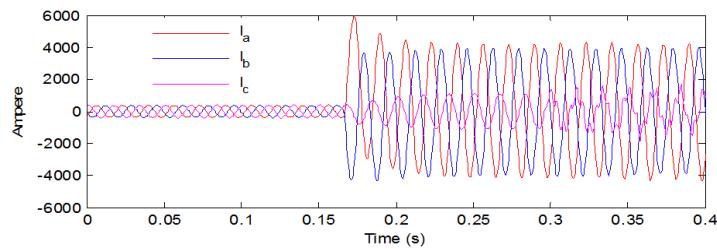


**Figure 23: Three-Phase Current at Bus-632 during LLG Fault in the Simultaneous Presence of Wind and Solar Power Generations**

The variations of the proposed fault index during double line to ground fault for all the three phases in the simultaneous presence of wind and solar PV power generations are shown in Figure 24. It is observed that the value of the fault index for all the three phases is below a threshold value (600) nearly 250 before the fault occurrence during the healthy condition. It can be observed that the value of fault indices is 2150 and 1950 for the faulty phases A and B respectively, after the occurrence of fault which is higher than the threshold value of 600. The value of fault index is less than 600 for the healthy phase-C. However, the fault index of the healthy phase also increases up to the value of 500 which is less than the threshold value. Hence, the healthy phase is clearly discriminated from the faulty phases. The high value of the fault index for the faulty phases will trip the respective relays to isolate the faulty section of the smart grid from healthy section.

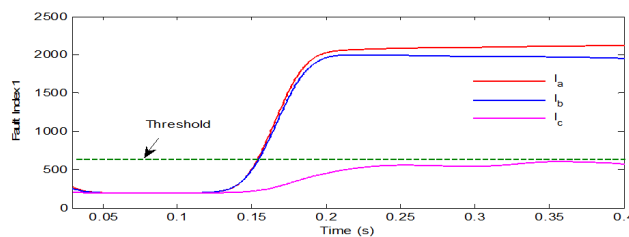


**Figure 24: Variation of Fault Indices for LLG Fault in the Simultaneous Presence of Wind and Solar Power Generations**

### 4.3.4. LLLG Fault

The three-phase fault involving ground in the simultaneous presence of wind and solar PV power generation has been created by simultaneous grounding all the three phases at the test location. The waveforms of currents of all the three phases captured at bus 632 on the test system before and after the fault incident are shown in Figure 25. It is observed that all the phases draw heavy currents after the fault occurrence. The magnitude of fault currents has increased by 1750 % of

the magnitude of current in healthy condition. These current waveforms are utilized to find the fault indices for the detection of the fault.

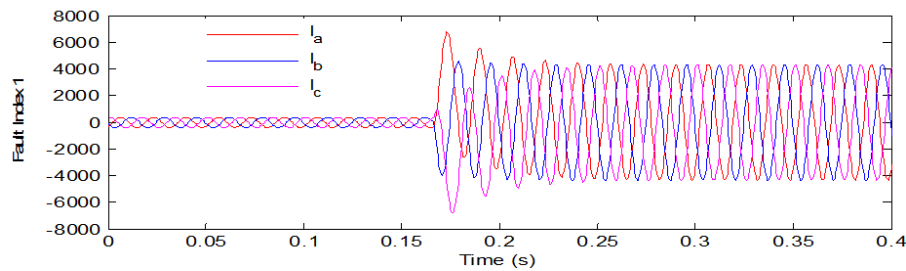


**Figure 25: Three-Phase Current at Bus-632 during LLLG Fault in the Simultaneous Presence of Wind and Solar Power Generations**

The variances of proposed fault indices during three-phase fault involving ground for all the three phases with the simultaneous presence of wind and solar PV power generations are shown in Figure 26. It is observed that the value of the fault index for all the phases is below a threshold value (600) nearly 250 before the fault occurrence during the healthy condition. It is also observed that the value of fault indices is 2150 for all the three phases after the occurrence of fault which is higher than the threshold value of 600. Hence, the three phase fault involving ground with simultaneous wind and solar PV power generations has been detected effectively and discriminated from other types of faults. The high value of fault index will trip the respective relays to isolate the faulty section of the smart grid.

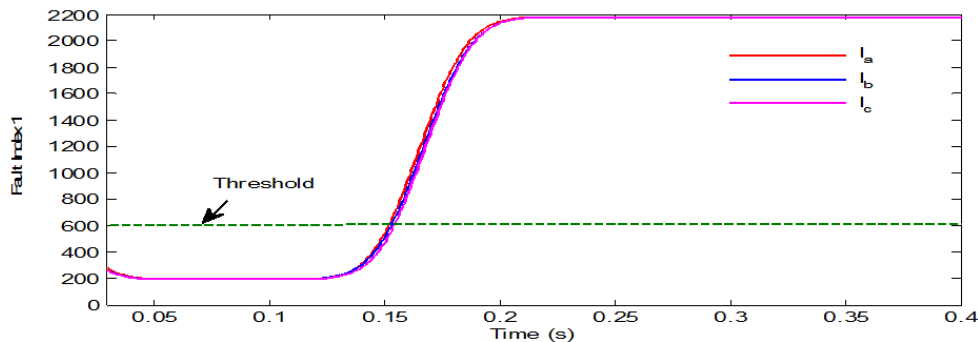


**Figure 26: Variation of Fault Indices for LLLG Fault in the Simultaneous Presence of Wind and Solar Power Generations**

### 5. DECISIONS TREE BASED CLASSIFICATION OF FAULTS

The power system faults occurring in the smart grid with RE sources have been classified using rule based decision tree. Decision rules are framed using the values of standard deviations calculated from the S-matrix obtained from the decomposition of current signals using Stockwell Transform. These values for all the types of faults are provided in the Table 2. The decision tree for the classification of faults in the smart grid along with the decision rules is shown in Figure 27.

Table 2

S. No.	Type of Fault	Values of Standard Deviations Obtained From S-Matrix		
		Phase-A	Phase-B	Phase-C
<b>A. Presence Solar PV Power Generation</b>				
1	LG	2.492	0.0875	0.9012
2	LL	3.549	3.541	0.1572
3	LLG	4.215	3.948	0.1802
4	LLLG	5.241	5.240	5.2428
<b>B. Presence of Wind Power Generation</b>				
1	LG	12.645	1.0842	1.9102
2	LL	13.561	13.613	1.1472
3	LLG	14.215	13.948	1.1713
4	LLLG	15.351	15.343	15.242
<b>C. Simultaneous Presence of Wind Solar PV Power Generation</b>				
1	LG	7.510	0.5875	0.9012
2	LL	8.549	8.572	0.8572
3	LLG	9.244	8.948	0.7802
4	LLLG	10.501	10.194	10.012

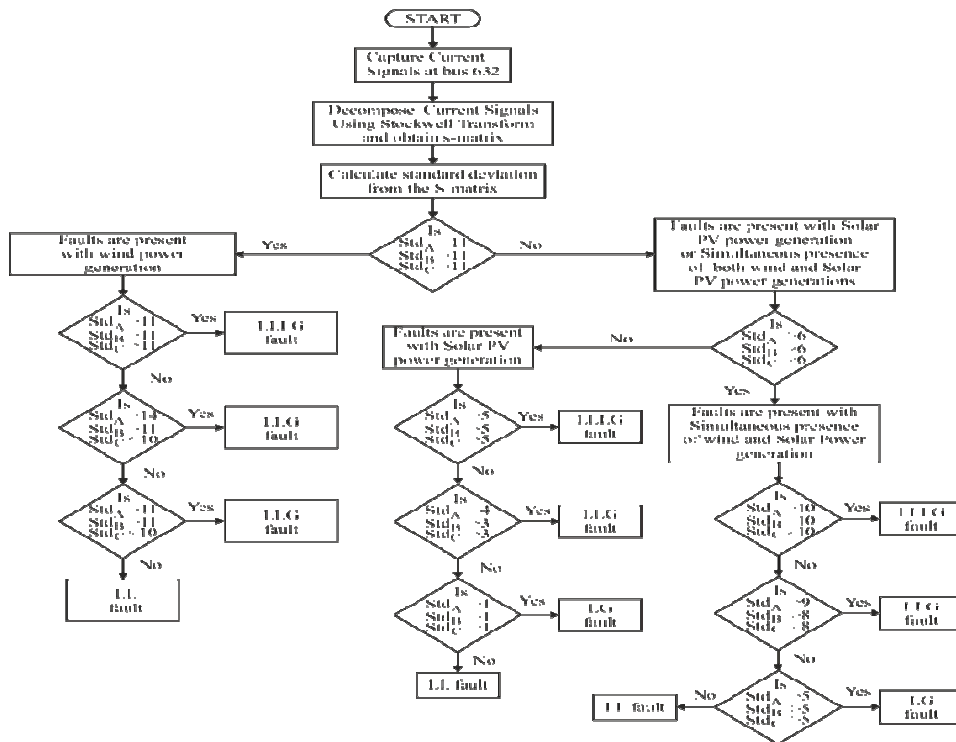


Figure 27: Decision Tree used for the Classification of Various Faults in the Smart Grid

6. PERFORMANCE OF PROPOSED TECHNIQUE

The performance of the proposed technique for the detection of faults in the smart grid has been evaluated by testing on the 100 data sets of each type of fault obtained by varying the various locations and fault impedance. The performance in terms of correctly classified and misclassified faults is shown in Table 3. It is observed that the efficiency of classification of faults have been achieved more than 98% in the presence of solar PV power generation, wind power generation and simultaneous presence of wind and solar PV power generations.

Table 3

S. No.	Type of Fault	Number of Correctly Classified Faults	Number of Misclassified Classified Faults	Percentage Efficiency (%)
<b>A. Presence Solar PV Power Generation</b>				
1	LG	100	0	100
2	LL	99	1	99
3	LLG	98	2	98
4	LLLG	100	0	100
<b>B. Presence of Wind Power Generation</b>				
1	LG	99	1	99
2	LL	97	3	97
3	LLG	97	3	97
4	LLLG	98	2	98
<b>C. Simultaneous Presence of Wind Solar PV Power Generations</b>				
1	LG	100	0	100
2	LL	98	2	98
3	LLG	98	2	98
4	LLLG	99	1	99
<b>Overall Efficiency (%)</b>				98.58

## 7. CONCLUSIONS

This paper presents a simple and effective technique for the detection and classification of power system faults in the smart grid. The proposed technique is based on the median of current values calculated from the S-matrix obtained by the decomposition of the current signals using Stockwell Transform. The various faults are detected and discriminated using a proposed fault index. Classification of the faults is carried out using the rule based decision tree. The rules for decision tree are framed using the standard deviations obtained from the S-matrix of the current signals. The proposed algorithm has been tested on the 100 data sets of each fault and an efficiency of classification more than 98 % has been achieved. The proposed study has been carried out using IEEE-13 bus test system modeled as smart grid in the MATLAB / Simulink environment.

## REFERENCES

1. Enrico De Santis, Lorenzo Livi, Alireza Sadeghian and Antonello Rizzi, "Modeling and recognition of smart grid faults by a combined approach of dissimilarity learning and one-class classification," *Neurocomputing*, Vol. 170, 2015, pp. 368–383.
2. James Hare, Xiaofang Shi, Shalabh Gupta and Ali Bazzi, "Fault diagnostics in smart micro-grids: A survey," *Renewable and Sustainable Energy Reviews*, Vol. 60, 2016, pp. 1114–1124.
3. Nan Wang, Visvakumar Aravinthan and Yanwu Ding, "Feeder-level fault detection and classification with multiple sensors: a smart grid scenario," *2014 IEEE Workshop on Statistical Signal Processing (SSP)*, 2014, pp. 37-40.
4. Kebina Manandhar, Xiaojun Cao, Fei Hu, and Yao Liu, "Detection of Faults and Attacks Including False Data Injection Attack in Smart Grid Using Kalman Filter," *IEEE Transactions on control of network systems*, Vol. 1, No. 4, December 2014, pp.370-379.

5. Mohamed M.A. Mahfouz, Mohamed A.H. El-Sayed, "Smart grid fault detection and classification with multi-distributed generation based on current signals approach," IET Generation, Transmission & Distribution, 2016, Vol. 10, Iss. 16, pp. 4040–4047.
6. N. Shahid, S. A. Aleem, I. H. Naqvi and N. Zaffar, "Support Vector Machine based Fault Detection and Classification in Smart Grids," GC'12 Workshop: Smart Grid Communications: Design for Performance," 2012, pp. 1526-1532.
7. Cheng-Guan Hou, Shih Chun Lin, Shih Tang Su, and Wei Ho Chung, "Fault tolerant quickest detection for power quality events in smart grid AMI networks," 2015 International Symposium on Intelligent Signal Processing and Communication Systems (ISPACS), November 9-12, 2015, pp. 159-163.
8. Huaiguang Jiang, Xiaoxiao Dai, David Wenzhong Gao, Jun Jason Zhang, Yingchen Zhang, and Eduard Muljadi, "Spatial-Temporal Synchrophasor Data Characterization and Analytics in Smart Grid Fault Detection, Identification, and Impact Causal Analysis," IEEE Transactions On Smart Grid, Vol. 7, No. 5, September 2016, pp. 225-2536.
9. Qian He, and Rick S. Blum, "Smart Grid Fault Detection Using Locally Optimum Unknown or Estimated Direction Hypothesis Test," ICSGCE 2011: 27–30 September 2011, Chengdu, China, Energy Procedia, Vol. 12, 2011, pp. 170-179.

